Pure Appl. Chem., Vol. 85, No. 11, pp. 2027–2049, 2013.
http://dx.doi.org/10.1351/PAC-CON-12-12-06

Thermodynamic description of Np(VI) solubility, hydrolysis, and redox behavior in dilute to concentrated alkaline NaCl solutions*

Xavier Gaona[1,‡], David Fellhauer[1,2], and Marcus Altmaier[1]

[1]Karlsruhe Institute of Technology, Institute for Nuclear Waste Disposal, P.O. Box 3640, 76021 Karlsruhe, Germany; [2]European Commission, Joint Research Centre, Institute for Transuranium Elements, P.O. Box 2340, 76125 Karlsruhe, Germany

Abstract: The solubility of Np(VI) was investigated in carbonate-free NaCl solutions (0.1 M ≤ I ≤ 5.0 M) at T = 22 ± 2 °C to derive thermodynamic properties of aqueous species and solid compounds formed under alkaline conditions. The experimentally derived solubility curves can be divided into four main regions: (I) ~7 ≤ pH_m ≤ ~9, showing a steep decrease in Np solubility with a slope (log [Np] vs. pH_m) of –3 or –2 (depending on NaCl concentration); (II) ~9 ≤ pH_m ≤ ~10.5, with a nearly pH-independent [Np]; (III) ~10.5 ≤ pH_m ≤ ~13.5, showing an increase in the solubility with a well-defined slope of +1. A region (IV) with a slope ≥ +2 was only observed at I ≥ 1.0 M NaCl and pH_m ≥ ~13.5. The solubility-controlling solid Np phases were characterized by X-ray diffraction (XRD), quantitative chemical analysis, thermogravimetric analysis and scanning electron microscopy-energy-dispersive spectrometry (SEM-EDS), confirming the presence of anhydrous $Na_2Np_2O_7$(cr) in regions II and III. The same solid phase was identified in region I except for the system in 0.1 M NaCl, where a $NpO_2(OH)_2 \cdot H_2O$(cr) phase predominates. XRD patterns of this solid phase show a very good agreement with that of metaschoepite ($UO_3 \cdot 2H_2O$), highlighting the similarities between Np(VI) and U(VI) with respect to solid phase formation and structure.

Based on the analysis of solubility data, solid phase characterization and chemical analogy with U(VI), the equilibrium reactions 0.5 $Na_2Np_2O_7$(cr) + 1.5 $H_2O \Leftrightarrow Na^+ + NpO_2(OH)_3^-$ and 0.5 $Na_2Np_2O_7$(cr) + 2.5 $H_2O \Leftrightarrow Na^+ + NpO_2(OH)_4^{2-} + H^+$ were identified as controlling Np(VI) solubility in regions II and III, respectively. The predominance of NpO_2^+ in the aqueous phase of region I (quantified by UV–vis/NIR) indicates the reductive dissolution of Np(VI) [either as $Na_2Np_2O_7$(cr) or $NpO_2(OH)_2 \cdot H_2O$(cr)] to $Np(V)_{aq}$. Oxidation to Np(VII) can explain the experimental observations in region IV, although it is not included in the chemical and thermodynamic models derived.

The conditional equilibrium constants determined from the solubility experiments at different ionic strengths were evaluated with both the specific ion interaction theory (SIT) and Pitzer approaches. Thermodynamic data for aqueous Np(VI) species [$NpO_2(OH)_3^-$ and $NpO_2(OH)_4^{2-}$] and solid compounds [$Na_2Np_2O_7$(cr) and $NpO_2(OH)_2 \cdot H_2O$(cr)] that are relevant under alkaline conditions were derived. These data are not currently included in the Nuclear Energy Agency-Thermochemical Database (NEA-TDB) compilation.

Keywords: hydrolysis; neptunium(VI); oxidizing redox conditions; Pitzer ion interaction model; solubility; thermodynamic description; specific ion interaction theory (SIT).

Pure Appl. Chem.* **85, 2027–2144 (2013). A collection of invited papers based on presentations at the 15th International Symposium on Solubility Phenomena and Related Equilibrium Processes (ISSP-15), Xining, China, 22–27 July 2012.
‡Corresponding author: E-mail: xavier.gaona@kit.edu

INTRODUCTION

Neptunium-237 is a long-lived ($t_{1/2} = 2.14 \times 10^6$ years) radionuclide relevant for the long-term safety assessment of nuclear waste repositories. In the context of high-level waste (HLW), ^{237}Np gains further relevance in the very long-term release scenarios (e.g., > 10 000 years) as key daughter product of ^{241}Am. Being a redox sensitive actinide, the alteration of geochemical redox conditions can induce changes in the redox state of Np and its chemical behavior that potentially impact the migration of this actinide from a repository into the biosphere. In this context, a detailed knowledge of Np solubility phenomena, aqueous speciation, and redox processes plays a key role in the assessment of an upper-limit concentration in the Np source term, as well as in the evaluation of sorption processes taking place in the near-to-far field of a nuclear waste repository.

NaCl- or $MgCl_2$-dominated salt brines are expected to form in the unlikely scenario of water intrusion in a salt rock repository [1–3]. On the other hand, cement-based wasteforms and repositories, which are foreseen in several countries for the disposal of low- and intermediate-level wastes, are characterized by the buffering of hyperalkaline pH conditions and presence of rather high Na^+ concentrations (~0.1 M) in the early stages of cement degradation [4].

The thermochemical database (TDB) project of the Nuclear Energy Agency (NEA) comprises the most comprehensive and authoritative selection of thermodynamic data currently available for actinides and fission products [5–8]. The selection of thermodynamic data within the NEA-TDB project relies upon exhaustive and critical reviews of the available scientific literature. Thermodynamic calculations based on the NEA-TDB selection for Np predict the predominance of Np(IV) for the highly reducing conditions expected for a deep geological repository as a result of the anoxic corrosion of iron. In this context, Np(V) is only expected to prevail in the early post-closure stages of a repository, as well as in the presence of oxidizing wasteforms. In the absence of complexing ligands other than water, Np(VI) would, according to the current NEA-TDB, only predominate at very acidic and oxidizing conditions, where it forms NpO_2^{2+}.

The formation of several Np(VI) hydrolysis species has been reported in the literature [9,10], although only $NpO_2(OH)^+$, $(NpO_2)_2(OH)_2^{2+}$, and $(NpO_2)_3(OH)_5^+$ are currently selected in the NEA-TDB. Based on the analogy concept for actinides in the same redox state [11,12] and considering the accurately described aqueous chemistry of U(VI), further hydrolysis products [i.e., $NpO_2(OH)_2(aq)$, $NpO_2(OH)_3^-$ and $NpO_2(OH)_4^{2-}$] would also be expected for Np(VI). Some of these species were considered likely to exist but were disregarded in the final NEA–TDB data selection, based on experimental shortcomings or poor data quality [5,13]. These species (primarily 1,3 and 1,4), however, will play an important role in alkaline to hyperalkaline conditions and influence Np solubility and speciation. Indeed, very recent spectroscopic [14,15] and sorption [16] studies have provided direct proof of the stability of Np(VI) aqueous species in the pH range of 10 to 13.5, well within the stability field of water, thus confirming the need to revisit the role and importance of Np(VI) for certain scenarios of nuclear waste disposal.

Several hydrated oxides and hydroxides of Np(VI) are reported in the literature [e.g., $NpO_3{\cdot}H_2O$(cr), $NpO_3{\cdot}2H_2O$, $NpO_3{\cdot}4H_2O$(am), $NpO_2(OH)_2$(cr), $NpO_2(OH)_2{\cdot}H_2O$] [17–21]. This points towards a complex system similar to the more comprehensively described U(VI) oxo-hydroxides [22]. On the basis of X-ray diffraction (XRD) patterns, several of these solids [$NpO_3{\cdot}2H_2O$, $NpO_2(OH)_2$(cr)] have been shown to be iso-structural with their U(VI) counterparts. Owing to this complexity, only log $*K^\circ_{s,0}$ for $NpO_3{\cdot}H_2O$(cr) was selected in [13], although it was considered likely that one or more of the other solids reported in the Np oxo-hydroxide system are similar in stability. In alkaline Na-rich environments and by analogy with U(VI), the precipitation of Na-neptunates is expected to occur. Four different Na–Np(VI) compounds are currently selected in the NEA–TDB [α-Na_2NpO_4, β-Na_2NpO_4, β-Na_4NpO_5, and $Na_2Np_2O_7$(cr)], although only $\Delta_f H^\circ_m$ data are available so far for these compounds. All these solids were thermally prepared by mixing NpO_2 and Na_2O at temperatures

between 670 and 1020 K [23,24], and their relevance as solubility-limiting solid phases in aqueous systems is generally questionable.

The redox potential and H^+ activity or concentration are the most important solution parameters defining the solubility and oxidation-state distribution of neptunium. A favorable approach to assess the complex redox chemistry of actinides is the use of "pe-pH diagrams", also known as E_h-pH or Pourbaix diagrams. This type of diagram shows the calculated pe-pH domains and stability fields of aqueous actinide species and solid compounds, provided that complete and accurate thermodynamic data are available for the corresponding actinide. Although kinetically hindered in the absence of catalytic surfaces, the upper (1) and lower (2) stability lines of water at $P[O_2(g)] = 1$ bar and $P[H_2(g)] = 1$, respectively, are conveniently used to delimit the region of interest in the pe-pH diagrams

$$0.5\ H_2O(l) \Leftrightarrow 0.25\ O_2(g) + H^+ + e^- \quad (1)$$

$$H^+ + e^- \Leftrightarrow 0.5\ H_2(g) \quad (2)$$

with $\log K°(1) = -20.77$ and $\log K°(2) = 0$. Analogous to the concept of neutral pH, Neck, Altmaier, and co-workers [25,26] defined the "redox neutrality" of a given aqueous solution as the E_h provided by partial pressures of $P[H_2(g)] = 2\ P[O_2(g)]$. Based upon the irreversible reaction $0.5\ H_2O(l) \Leftrightarrow 0.25\ O_2(g) + 0.5\ H_2(g)$ with $\log K° = \log K°(1) + \log K°(2) = -20.77$, it is possible to calculate the hypothetical values of $P[H_2(g)] = 2P[O_2(g)] = 2.5 \times 10^{-28}$ bar, and therefore the pH-dependent "redox neutral" line as pH + pe = 13.8. The "redox neutral" line can neither be measured nor expected in "real" systems, but remains as a theoretical construct that is very useful in separating the reducing and oxidizing conditions within a pe-pH diagram.

In order to improve the present lack of understanding and limited thermodynamic description of Np(VI) in alkaline systems, solubility experiments in combination with spectroscopy and a detailed solid phase characterization were performed. These results were used to derive thermodynamic properties of Np(VI) aqueous species and solid compounds formed in alkaline NaCl solutions. The systematic variation of NaCl concentration in the experimental series results in a complete picture of experimental Np solubility limits from dilute to concentrated NaCl solutions, and offers a sufficient basis for deriving reliable thermodynamic data and ion interaction parameters. The "specific ion interaction theory" (SIT) [27] and the Pitzer ion interaction model [28,29] were both used to derive equilibrium constants at $I = 0$ and the corresponding activity model parameters.

EXPERIMENTAL

Chemicals

NaCl (p.a.), NaOH (Titrisol®), and HCl (Titrisol) were purchased from Merck. Carbonate impurities in 1 M NaOH (Titrisol) were quantified as $3.1 \pm 0.2 \times 10^{-5}$ M. NaClO was prepared by flushing $Cl_2(g)$ through a 1 M NaOH solution at 0 °C under an Ar atmosphere to minimize carbonate impurities (found to contaminate commercially available NaClO). The final concentration of NaClO was 0.71 ± 0.04 M in ~0.7 M NaOH. All solutions were prepared with ultrapure water purified with a Milli-Q-academic (Millipore) apparatus and purged with Ar before use. All solutions and samples were prepared, stored, and handled inside an inert gas (Ar) glovebox at 22 ± 2 °C.

Solid phase preparation and characterization. Solubility measurements

A radiochemically well characterized Np(V) stock solution in ~0.8 M HCl containing about 200 mg ^{237}Np was oxidized to Np(VI) on a platinum anode at E_{anode} ~ +1.3 V vs. SHE. The redox purity of the Np(VI) stock solution was confirmed by ultraviolet–visible near-infrared spectroscopy (UV–vis/NIR) with a high-resolution UV–vis/NIR spectrometer Cary 5 (Varian, USA). The slow addition of the

Np(VI) stock solution to an alkaline 2.5 M NaCl solution (pH_m ~12) with 5×10^{-3} M NaClO resulted in the immediate precipitation of a brownish solid phase. After two months of equilibration in the same matrix solution, the solid phase was characterized by XRD, chemical analysis and scanning electron microscopy-energy-dispersive spectrometry (SEM-EDS). For this purpose, a small amount (~1 mg) of the solid Np phase was taken from solution and washed 5 times with ethanol (2 mL) under an Ar-atmosphere to remove the matrix solution (NaCl). The largest fraction of the resulting solid was used for XRD analysis with a Bruker D8 Advance diffractometer (Cu Kα radiation) equipped with a Sol-X detector. XRD data were collected within $5º \leq 2\Theta \leq 60º$, with a step size of 0.04º and 6 s accumulation time per step. After the XRD measurement, the solid phase was dissolved in 2 % HNO_3, and analyzed for Np and Na concentration by liquid scintillation counting (LSC, 1220 Quantulus instrument, Perkin Elmer) and inductively coupled plasma–optical emission spectrometry (ICP-OES, Optima 2000, Perkin Elmer), respectively. Samples for LSC analysis were mixed with 10 mL of LSC-cocktail Ultima Gold XR (Perkin-Elmer), resulting in a detection limit of ~5×10^{-9} M for ^{237}Np (α-radiation measured after α/β-discrimination of the counts from the daughter nuclide ^{233}Pa). The fraction of the solid not used for XRD analysis was characterized by SEM-EDS with a CamScan FE44 SEM equipped with a Noran EDS unit.

This well-characterized solid was then distributed to 5 experimental series of increasing ionic strength (0.1, 0.5, 1.0, 2.5, and 5.0 M NaCl), with $7 \leq pH_m \leq 14.5$, giving a total of 35 independent batch samples. The amount of Np in each sample was ~5 mg. Oxidizing conditions required for the stabilization of Np(VI) were achieved by addition of 5×10^{-3} M NaClO. Previous studies have reported the possible complexation of NaClO to Pu(VI) [30] and U(VI) [31] under near-neutral to slightly alkaline pH conditions. Because of relevant experimental shortcomings, the NEA-TDB did not consider any of the proposed complexes in the thermodynamic data selection [5,13]. In order to assess a potential impact of hypochlorite complexation on Np(VI) solubility and speciation in the present study, four additional samples ([NaClO] = 5×10^{-2} M and 5×10^{-4} M; I = 0.1 M and 5.0 M NaCl; pH_m ~12.5–13) were prepared.

The Np(VI) solubility batch samples were equilibrated for up to ~450 days, with pH, E_h, and [Np] being systematically monitored during this period. The aqueous concentration of Np was measured after 10 kD ultrafiltration (Pall Life Sciences) by LSC. After ensuring equilibrium conditions (constant [Np] and pH_m), the solubility experiments were terminated and the solid phase was characterized by XRD, chemical analysis, and SEM-EDS in selected samples. Samples with [Np] > 1×10^{-5} M (in the near-neutral pH range and $pH_m \geq 13.5$) were centrifuged in the glovebox at 4020 *g* to remove suspended particles of the solid phase, and a UV–vis/NIR spectrum of the supernatant was recorded between 300 nm $\leq \lambda \leq$ 1400 nm to assess the speciation of Np in the aqueous phase.

The number of waters of hydration in well-defined solids was determined by thermogravimetric analysis using a Netzsch STA 409 C/CD apparatus operated under an Ar atmosphere. About 100 mg of the selected neptunate phase was prepared following the same protocol used for XRD sample preparation. The temperature program included a preliminary step of 10 min at 80 °C to ensure the complete evaporation of the (potentially) remaining ethanol, followed by a steady heating at 5 °C/min up to 800 °C, where the temperature was kept for 2 h.

Measurements of pH and E_h

A combination glass pH electrode (type ROSS, Orion), freshly calibrated against dilute standard pH buffers (pH 1–13, Merck), was used to determine the molal H^+ concentration, m_{H^+} (with $pH_m = -\log m_{H^+}$). In salt solutions of ionic strength $I \geq 0.1$ mol·kg^{-1}, the measured pH value (pH_{exp}) is an operational apparent value related to m_{H^+} by $pH_m = pH_{exp} + A_m$, where A_m is given as a function of the NaCl concentration [1]. This approach is equivalent to calibrating the electrode vs. standard samples with fixed proton concentration at constant background electrolyte concentrations and relates the potential

measured in the samples to the proton concentrations on a molal scale. In NaCl–NaOH solutions with $[OH^-] > 0.03$ M, the H^+ concentration was calculated from the given $[OH^-]$ and the conditional ion product of water.

Redox potentials were measured with a Pt combination electrode with Ag/AgCl reference system (Metrohm) and converted into E_h vs. standard hydrogen electrode (SHE) by correcting for the potential of the Ag/AgCl reference electrode at 3 M KCl and 22 °C. The performance of the redox electrode was tested with a standard redox buffer solution (Schott, +640 mV vs. Ag/AgCl) and provided readings within ±10 mV of the certified value.

As in pH measurements with combination glass electrodes, liquid junction potentials result at the diaphragm of the Pt combination electrode due to differences in the mobility of ions present in the internal reference solution (3 M KCl) and in the background electrolyte of the sample. Liquid junction potentials calculated for the experimental conditions in this study remain well below 20 mV even in the most drastic conditions investigated (1 M NaOH + 4 M NaCl). Given the uncertainty in the E_h measurements considered in this work (±50 mV, in contrast to pH measurements, ±3 mV), E_h values are reported without further correction.

RESULTS AND DISCUSSION

Np(VI) solubility data and evolution of redox conditions

The Np(VI) solubility data determined in the 0.1, 0.5, 1.0, 2.5, and 5.0 M NaCl solutions in the presence of NaClO are shown in Figs. 1a–e. Experimental molar concentrations of Np (M, $mol \cdot L^{-1}$) determined by LSC are transformed to molal units (m, $mol \cdot kg^{-1}$ H_2O) using the conversion factors reported in [5]. Samples for which solid phase characterization and/or UV–vis/NIR analysis of the supernatant solution were performed are indicated. Four different regions/trends can be identified:

- **Region I: ~7 ≤ pH_m ≤ ~9** A steep decrease in the solubility curve is observed. The slope (log [Np] vs. pH_m) is approximately –3 for samples in 0.5, 1.0, 2.5, and 5.0 M NaCl, but increases to about –2 for 0.1 M NaCl. A significant kinetic trend was observed in this region, resulting in an increase of [Np] and pH_m with time.
- **Region II: ~9 ≤ pH_m ≤ ~10.5** Showing a nearly pH-independent [Np]. This region represents the minimum [Np] of the solubility curve (10^{-7}–10^{-8} M).
- **Region III: ~10.5 ≤ pH_m ≤ ~13.5** An increase in the solubility with a well-defined slope of +1 is observed.
- **Region IV: pH_m ≥ ~13.5** A region with a steeper increase in the solubility curve (slope ≥ +2) than observed for Region III.

Figures 1f–j also show the E_h values measured in all samples within the timeframe of the solubility experiment. In all the systems, NaClO initially creates very oxidizing conditions, well above the border of water oxidation. With time, however, NaClO starts to degrade and E_h decreases. This degradation process is enhanced at low pH_m and high ionic strength. The decrease in E_h has no effect on Np(VI) solubility except in the near-neutral pH range (region I), where it is accompanied by an increase in [Np] and pH_m. The time-dependence of E_h, pH_m, and [Np] is shown in Fig. 2 for selected samples in I = 0.1, 0.5, and 5.0 M NaCl.

The drastic drop of E_h in the near-neutral pH region (from pe ~18 to pe ~6) leads to unbuffered "redox neutral" systems after long equilibration times of ~400 days (Fig. 2, upper left). These E_h values (measured after the degradation of NaClO) are considered unreliable, given the lack of any further redox couple in sufficient concentration (> 10^{-6} M, see [32,33]) as to be properly detected with a Pt combination electrode.

The increase of [Np] accompanying the decrease of E_h in region I is related to the reduction of Np(VI) to Np(V) in the aqueous phase. Although no absorption bands are known for Np(VI) hydroly-

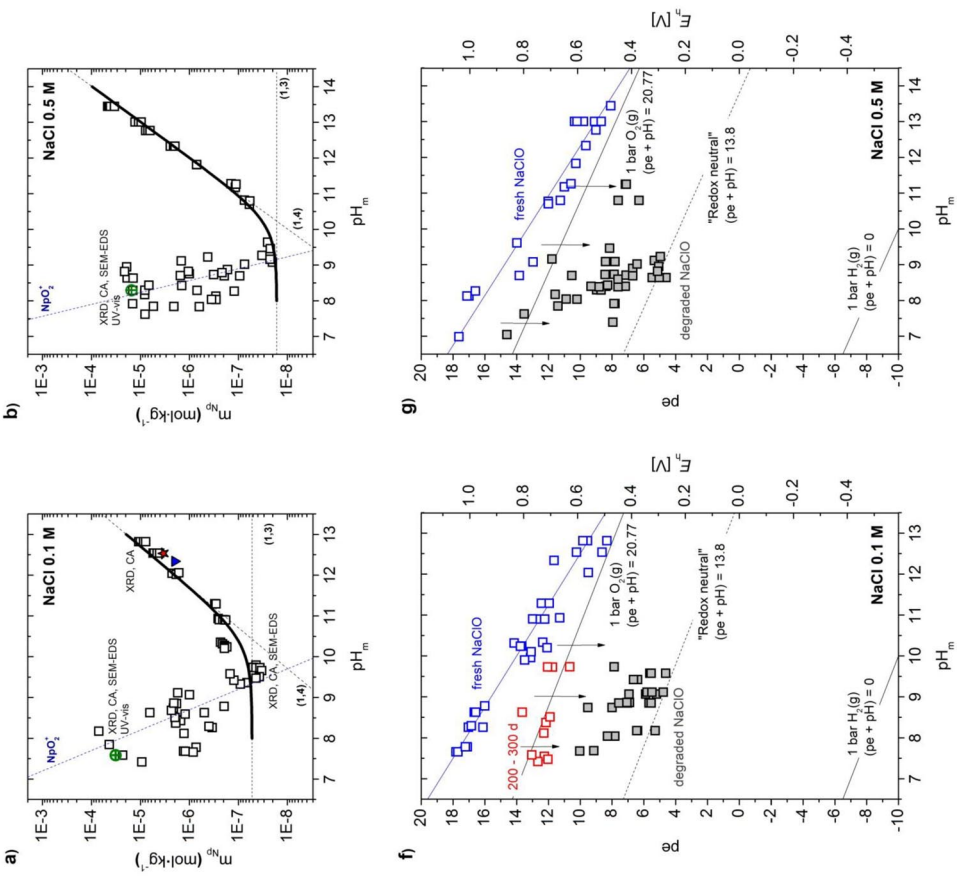

Fig. 1 (a–e) Solubility of Np(VI) in 0.1, 0.5, 1.0, 2.5, and 5.0 M NaCl (m_{NaCl} = 0.10, 0.51, 1.02, 2.64, and 5.61 mol·kg^{-1}); experimental data (molal scale) and Pitzer model calculations (thick lines: total Np concentrations, thin dashed lines: contributions of the different species). Symbols ★ and ▼ correspond to samples prepared with 5×10^{-4} M and 5×10^{-2} M NaClO, respectively. Symbol ⊕ indicates the concentration of NpO_2^+ measured by UV–vis/NIR. (f–j) E_h values measured for the solubility samples at $1 \le t$ [days] ≤ 450.

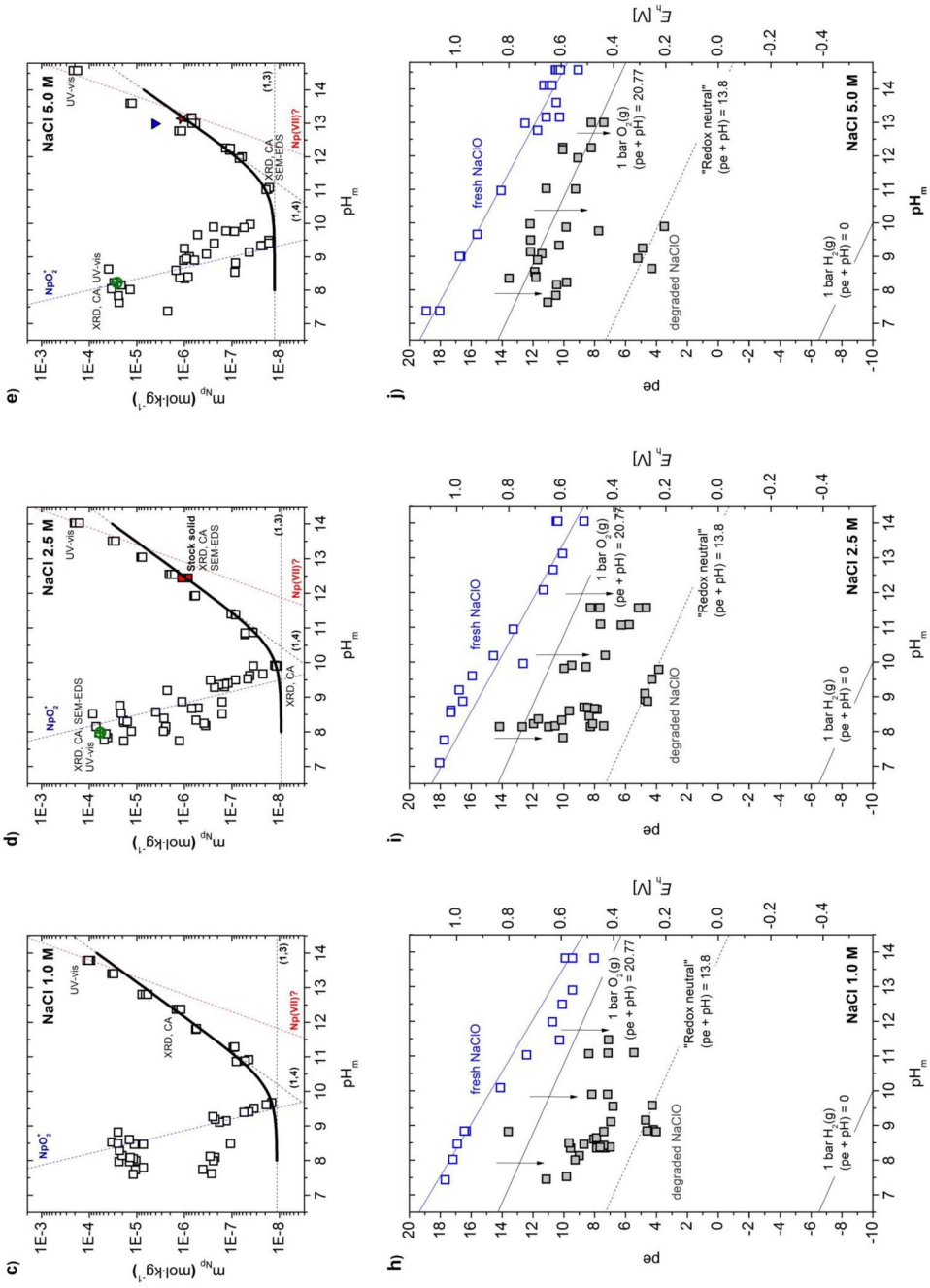

Fig. 1 (Continued).

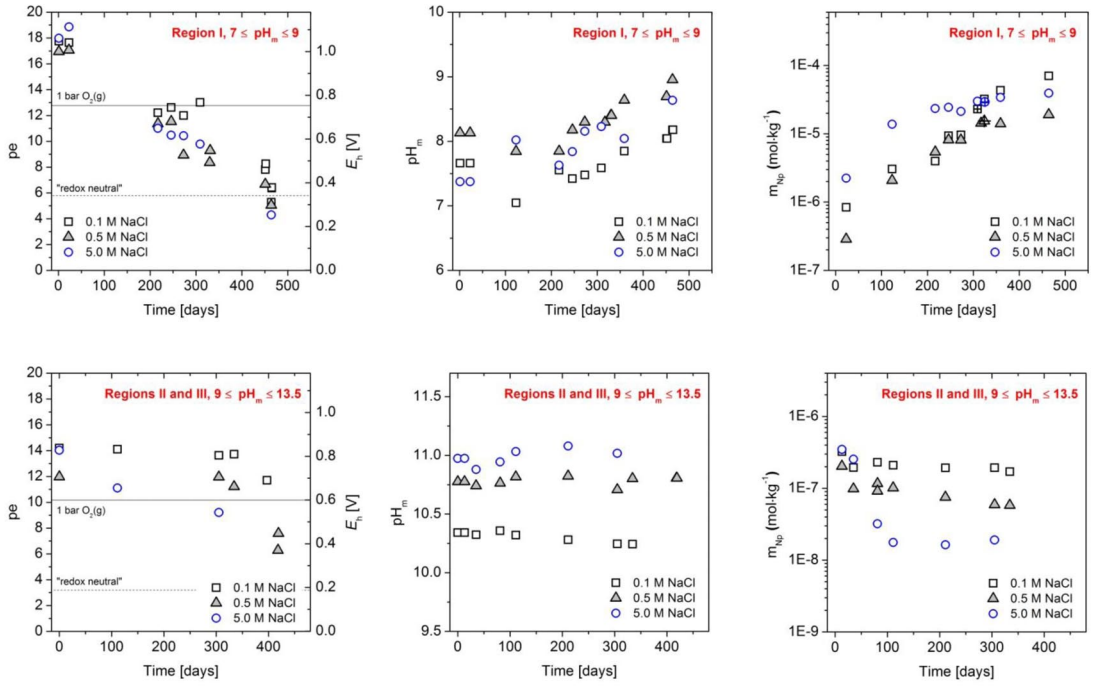

Fig. 2 Time-dependence of E_h, pH_m, and total [Np] for selected samples in regions I–III at I = 0.1, 0.5, and 5.0 M NaCl. Symbols ⊞, ⧋, and ⊕ corresponding to [NpO_2^+] determined by UV–vis/NIR for samples in 0.1, 0.5, and 5.0 M, respectively (see also Figs. 1 and 3).

sis species, the UV–vis/NIR analysis of the supernatant solution in the near–neutral pH samples (region I) unequivocally indicates the presence of NpO_2^+ (λ = 980–981 nm) for all I conditions considered in the study (Fig. 3). The quantification of [NpO_2^+] based on the experimental peak height and the corresponding molar extinction coefficient (ε_{max}= 395 ± 5 L·mol^{-1}·cm^{-1} [34]) is in very good agreement with [Np] determined by LSC, thus confirming the predominance of NpO_2^+ and absence of Np(VI) in the aqueous phase. Data on [NpO_2^+] resulting from UV–vis/NIR analysis are included in Figs. 1 and 2 for comparison.

Despite the confirmed formation and predominance of NpO_2^+ in the aqueous phase under near-neutral pH conditions, the comparison of our results with Np(V) solubility data in analogous NaCl [35] and $NaClO_4$ [36] solutions suggests that solubility is not controlled by a Np(V) solid phase. Hence, Np concentration in region I is between 1 and 3 orders of magnitude below the solubility of NpO_2OH(am) reported for the same pH and I conditions. Note also that [35] only observed the formation of Na–Np(V) compounds at $pH_m \geq 11.8$ and $I \geq 1.0$ M NaCl.

In contrast, the XRD characterization of the solid phases in region I clearly shows that these remain as Np(VI) in the form of $NpO_2(OH)_2 \cdot H_2O$(cr) (I = 0.1 M NaCl) or $Na_2Np_2O_7$(cr) (0.5 ≤ I ≤ 5.0 M NaCl) (see next section). The increase of both pH_m and [Np] can be thus explained by the reductive dissolution of the Np(VI) solid phase

$$NpO_2(OH)_2 \cdot H_2O(cr) + e^- \Leftrightarrow NpO_2^+ + 2\ OH^- + H_2O \qquad (0.1\ M\ NaCl) \qquad (3)$$

$$0.5\ Na_2Np_2O_7(cr) + 1.5\ H_2O + e^- \Leftrightarrow Na^+ + NpO_2^+ + 3\ OH^- \qquad (0.5–5.0\ M\ NaCl) \qquad (4)$$

Most of the thermodynamic description of Np(VI) aqueous species and solid compounds reported in the following sections are based on experimental data in regions II and III. Equilibrium conditions are rapidly attained within days in both regions, as confirmed by the stable [Np] and pH_m readings

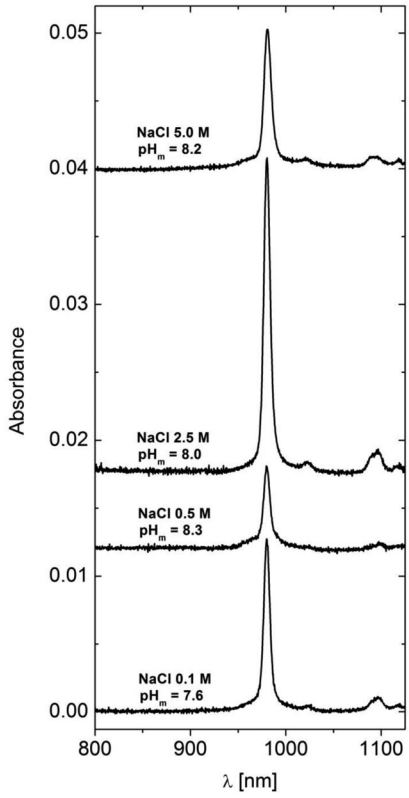

Fig. 3 UV–vis/NIR spectra of selected samples in region I with $0.1 \le I \le 5.0$ M NaCl. All spectra collected at t ~325 days. A deliberate offset was added to the absorbance of each sample to facilitate the comparison between spectra.

observed within the period of 5–400 days (see Fig. 2). A solubility reaction involving the release of one proton dominates region III over a [H^+]- and [Np]-range of (in some systems) more than 3 orders of magnitude. A very similar trend observed for the solubility of U(VI) under analogous experimental conditions was attributed to the equilibrium reaction 0.5 $Na_2U_2O_7 \cdot H_2O + 2\ H_2O \Leftrightarrow Na^+ + UO_2(OH)_4^{2-} + H^+$ (see [37] and Appendix).

The pH independence of [Np] in region II is clear but restricted to a narrow pH window, compared to U(VI) (see Appendix). This is mostly caused by the prominent increase of Np solubility in region I, which takes place at pH_m ~9–10 in contrast to pH_m ~7–8 observed for U(VI). This observation likely indicates that the equilibrium reaction governing the solubility phenomena in region I is different for these actinides.

No significant effect of hypochlorite complexation on Np(VI) solubility is observed in region III at $I = 0.1$ M for [NaClO] = 5×10^{-4} M (Fig. 1, ★), 5×10^{-3} M and 5×10^{-2} M (Fig. 1, ▼). At I = 5.0 M, a slight increase in Np(VI) solubility (~0.3 log-units) occurs for [NaClO] = 5×10^{-2} M, indicating that a highly charged Np(VI)–OH–ClO species may have formed at high NaClO concentrations. These observations confirm that, at the concentration level used in this study (5×10^{-3} M), NaClO does not have any significant effect on Np(VI) solubility and aqueous speciation and can be used to stabilize the hexavalent Np oxidation state without further impacting Np solution chemistry.

The steeper increase in the solubility observed in region IV can be only explained by the formation of a new aqueous species. Considering the behavior of this new species with respect to ionic strength and pH, it can be safely postulated that the aqueous species forming in region IV has a higher

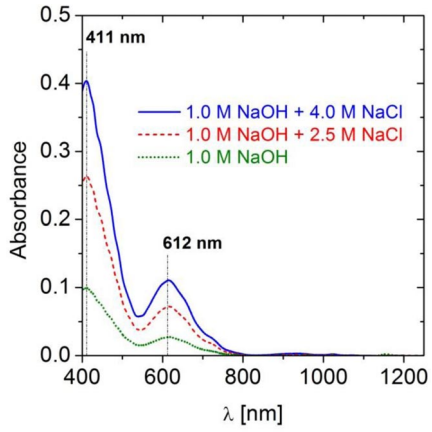

Fig. 4 UV–vis/NIR spectra of selected samples in region IV with $1.0 \leq I \leq 5.0$ M NaCl–NaOH. All spectra collected at t ~60 days.

charge and/or number of OH-ligands than the Np(VI) species prevailing in region III. The formation of the new species is accompanied by a visible change in the supernatant solution, which acquired a bright green color. As shown in Fig. 4, two absorption bands in the visible region with maxima at 411 and 612 nm are unequivocally identified in the UV–vis/NIR spectra collected for samples in 1.0 M NaOH at three ionic strengths (1.0, 2.5, and 5.0 M NaCl–NaOH). Molar extinction coefficients determined for both bands are 1490 ± 30 and 380 ± 20 $L \cdot mol^{-1} \cdot cm^{-1}$.

Several studies available in the literature have reported the formation of Np(VII) under hyperalkaline and very oxidizing conditions. The pioneering work by Spitsyn and co-workers [38] exhaustively assessed the oxidation of Np(VI) to Np(VII) under hyperalkaline conditions (0.25–1.0 M NaOH/KOH) in different oxidizing media (XeO_3, Na_4XeO_6, $K_2S_2O_8$, KIO_4, $NaBiO_3$, KClO, and KBrO). Most of the experiments were conducted at $T \geq 50$ °C. Two characteristic bands at 410 and 625 nm were observed in the greenish solutions formed after oxidation. The molar extinction coefficients of these peaks in 1 M KOH were quantified as 1350 and 385 $L \cdot mol^{-1} \cdot cm^{-1}$, respectively. Similar spectroscopic features were observed by Shilov and co-workers [39] for the oxidation of Np(VI) with ozone at $T = 22$–23 °C. Advanced spectroscopic techniques (EXAFS, XANES) as well as density functional theory (DFT) and NMR studies have recently helped to identify the structure of Np(VII) in alkaline solutions, which is reported as $NpO_4(OH)_2^{3-}$ [40–43]. Nevertheless, a definitive proof of concept relating fingerprint-based UV–vis/NIR interpretation with Np(VII) structural data available from EXAFS studies is so far lacking in the literature.

The increase in solubility with slope ≥ +2 observed in region IV can be also interpreted with the formation of $Np^{VI}O_2(OH)_5^{3-}$ in equilibrium with $Na_2Np_2O_7$(cr). The existence of the analogous monomeric pentahydroxo complex of U(VI) ($UO_2(OH)_5^{3-}$) was largely discussed in the NEA-TDB update [5] based on the few experimental studies available in the literature. The predominance of $UO_2(OH)_4^{2-}$ rather than $UO_2(OH)_5^{3-}$ as limiting hydrolysis complex was favored in the final data selection, although the formation of the latter was hinted by spectroscopic studies [44,45].

The formation of either $Np^{VII}O_4(OH)_3^{3-}$ or $Np^{VI}O_2(OH)_5^{3-}$ can adequately explain the experimental observations obtained in this work (region IV in solubility data). Although the former appears more likely on the basis of UV–vis/NIR observations, both remain as speculative hypotheses to be further confirmed by dedicated spectroscopic studies under analogous experimental conditions which are currently under way at KIT-INE.

Solid phase characterization

Well-defined and sharp XRD peak features obtained in all samples indicate a high degree of crystallinity in the solid phases. The same XRD patterns were found for the initial Np(VI) solid phase (formed in 2.5 M NaCl, pH_m ~12) and selected solid samples in regions II and III (Fig. 5a) at the end of the experiments. This confirms that the same solid phase is controlling the solubility in both regions, and that this phase remained stable within the timeframe of the study. The XRD pattern of the solid neptunate was successfully identified as $Na_2Np_2O_7$(cr) (JCPDS File 13-1231). The structure was originally characterized by Keller and co-workers [46], who synthesized this solid phase by mixing NpO_2:Na_2O with a 2:1 ratio at 400 °C.

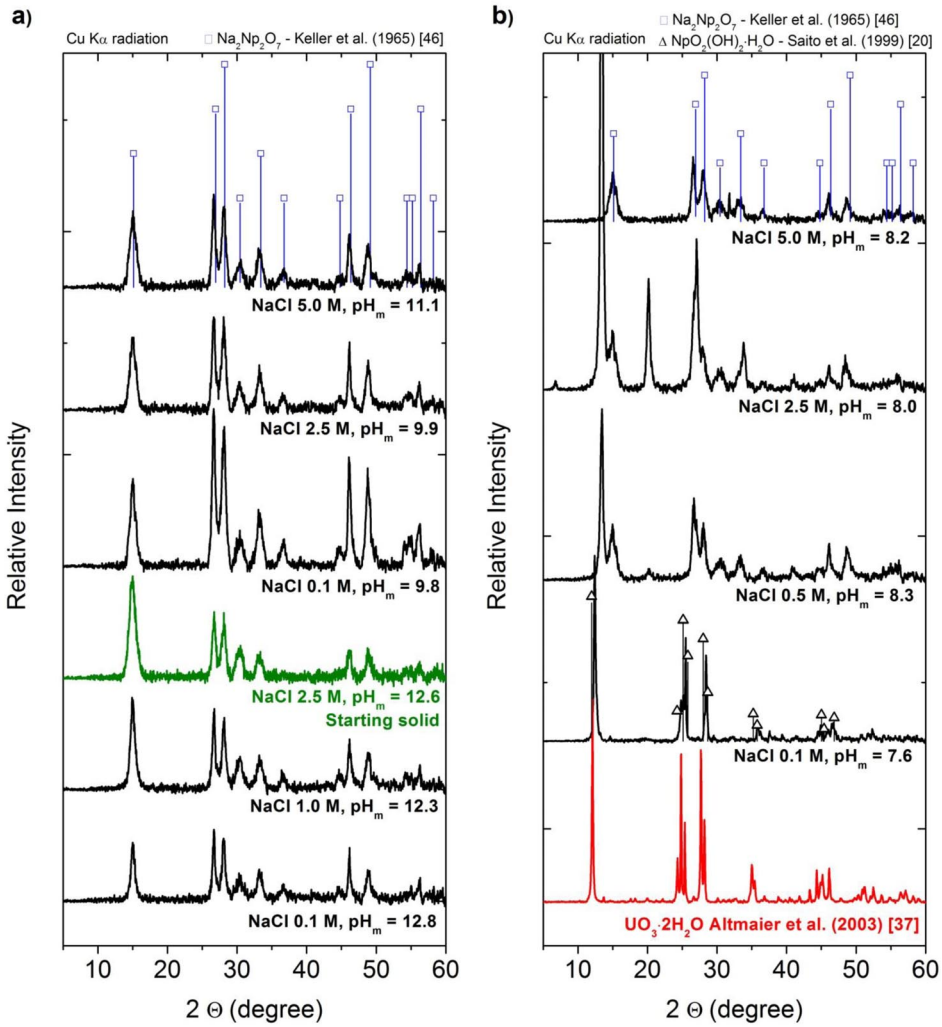

Fig. 5 XRD spectra of selected solid phases from solubility experiments in regions II/III (a) and I (b). Squares and triangles mark peak positions and relative intensities reported for $Na_2Np_2O_7$(cr) [46] and $NpO_2(OH)_2 \cdot H_2O$(cr) [20], respectively. Red XRD spectrum in the bottom right corresponds to the U(VI) solid phase $UO_3 \cdot 2H_2O$ stable for $pH_m \leq 7$ [37].

A more complex behavior is observed under near-neutral to slightly alkaline pH conditions (region I, Fig. 5b). The $Na_2Np_2O_7$(cr) phase predominates in 5.0 M NaCl. This same phase is identified in 0.5 and 2.5 M NaCl and pH_m = 8.0–8.3, although they coexist with an undefined solid phase with intensive peaks at 2Θ = 13.45 and 20.18 degrees. A new crystalline solid Np(VI) phase forms in 0.1 M NaCl, whose XRD pattern has the very same XRD fingerprint as metaschoepite ($UO_3 \cdot 2H_2O$, JCPDS File 43-0364) in the case of U(VI). Although not currently included in the JCPDS XRD database, this compound has been identified as $NpO_2(OH)_2 \cdot H_2O$(cr) based on the work by Saito and coworkers [20].

To gain further information on the solubility-limiting solid Np phases, the Na:Np ratio of selected solid phases was determined by chemical analysis and SEM-EDS (Table 1). Experimental error in chemical analysis by LSC and ICP-OES can be safely considered ≤ 10 %, whereas uncertainty associated with SEM-EDS for a given sample lies typically within 20–40 % (as standard deviation of 10 individual measurements). SEM-EDS is also more sensitive to eventual heterogeneities of the samples (e.g., mixture of solid phases). Both methods result in a Na:Np ratio ~1 for solid phases in regions II and III, confirming the stoichiometry derived from XRD analyses. A significant discrepancy between the chemical analysis and SEM-EDS is observed for the Na:Np ratio of solid samples in region I (mostly at 0.5 and 2.5 M NaCl). Given the higher accuracy of chemical analysis, we use these values in the following discussion.

Table 1 Ratio Na:Np in the solid phase determined by chemical analysis and SEM-EDS.

Region	I [M]	pH_m	Na:Np (chemical analysis)	Na:Np (SEM-EDS)
I	0.1	7.6	0.2	0.2
	0.5	8.3	0.7	1.1
	2.5	8.0	0.7	1.0
	5.0	8.2	1.4	n.m.
II	0.1	9.8	1.0	1.2
	2.5	9.9	1.0	n.m.
	5.0	11.1	1.2	1.3
III	0.1	12.8	1.0	n.m.
	1.0	12.3	0.9	n.m.
	2.5[a]	12.6	0.9	1.0

[a]Starting solid.
n.m. not measured.

The decrease in the Na content of the solid phases observed in region I for the sequence 5.0 M → 0.1 M NaCl is in good agreement with the XRD data, which shows the predominance of crystalline $Na_2Np_2O_7$(cr) and $NpO_2(OH)_2 \cdot H_2O$(cr) in 5.0 and 0.1 M NaCl, respectively. Despite the presence of an unidentified solid phase in 0.5 and 2.5 M NaCl [coexisting with $Na_2Np_2O_7$(cr)], the equilibrium reactions controlling the solubility of Np in region I can be simplified as

$$0.5\ Na_2Np_2O_7(cr) + 1.5\ H_2O + H^+ \Leftrightarrow Np(V)_{aq} \Leftrightarrow NpO_2(OH)_2 \cdot H_2O(cr) + Na^+ \quad (5)$$

As previously observed for U(VI) (see [37] and Appendix), the phase transformation between $Na_2Np_2O_7$(cr) and $NpO_2(OH)_2 \cdot H_2O$(cr) takes place within a narrow pH range. From reaction 5, it is apparent that the transformation of one solid phase into another depends only on $[Na^+]$ and $[H^+]$. This relationship will be used in the following evaluation to derive thermodynamic properties of $NpO_2(OH)_2 \cdot H_2O$(cr) and $Na_2Np_2O_7$(cr).

Thermogravimetric and differential thermal analysis (TG-DTA) was performed on the solid phase formed in regions II and III, where XRD, quantitative chemical analysis, and SEM-EDS previously confirmed the predominance of a single-crystalline phase (see above). About 100 mg of this solid phase collected from different solubility samples in these regions were analyzed with the temperature program described in the experimental section (T_{max} = 800 °C). A minor loss of mass of ~0.4 % is observed in the TG analysis, confirming a very anhydrous character of the solid phase with neither crystalline water nor hydroxyl groups present. Although unexpected for an actinide solid phase precipitated from aqueous solution at 25 °C, this result is fully consistent with the sharp XRD features obtained for this compound, and there is very good agreement with the XRD spectra reported by Keller and co-workers [46] for a Na-neptunate solid phase synthesized at 400 °C.

Chemical and thermodynamic models

The development of a correct chemical model (set of chemical reactions defining the aqueous system) for the behavior of Np(VI) in alkaline conditions is based upon solid and aqueous phase characterization, slope analysis of the solubility curves, and chemical analogy with U(VI). This step sets the basis for the subsequent evaluation of thermodynamic and activity model parameters.

Np(VI) hydrolysis species in equilibrium with $Na_2Np_2O_7$(cr)

All calculations, equilibrium constants, and illustrations shown in this section are given on the molal concentration scale. The values of water activity a_w at different NaCl concentrations are taken from [5]. Both SIT [5,27] and Pitzer [28,29] approaches are used for deriving log K values at I = 0 and extracting the corresponding ion interaction parameters. Note here that it is of high importance to use thermodynamic parameters consistently: equilibrium constants at I = 0 derived within the Pitzer approach are to be used with the corresponding Pitzer model parameters to calculate activity coefficients; the use of SIT data likewise demands a consistent approach.

The anionic hydrolysis species $AnO_2(OH)_3^-$ and $AnO_2(OH)_4^{2-}$ are known to dominate the aqueous speciation of U(VI) above pH_m ~7. Based on the expected analogy among actinides of the same redox state, the formation of the same aqueous species is expected for both Np(VI) and Pu(VI). Considering the predominance of the solid $Na_2Np_2O_7$(cr) and accounting for the slope analysis detailed above, the chemical reactions 6 and 7 control the solubility of Np(VI) in regions II and III

$$0.5\ Na_2Np_2O_7(cr) + 1.5\ H_2O \Leftrightarrow Na^+ + NpO_2(OH)_3^- \quad (6)$$

$$0.5\ Na_2Np_2O_7(cr) + 2.5\ H_2O \Leftrightarrow Na^+ + NpO_2(OH)_4^{2-} + H^+ \quad (7)$$

with

$$\log\ {}^*K'_{s,(1,3)} = \log\ [NpO_2(OH)_3^-] + \log\ [Na^+] \quad (8)$$

$$\log\ {}^*K^\circ_{s,(1,3)} = \log\ {}^*K'_{s,(1,3)} + \log\ \gamma_{(1,3)} + \log\ \gamma_{Na^+} - 1.5\ \log\ a_w \quad (9)$$

and

$$\log\ {}^*K'_{s,(1,4)} = \log\ [NpO_2(OH)_4^{2-}] + \log\ [Na^+] + \log\ [H^+] \quad (10)$$

$$\log\ {}^*K^\circ_{s,(1,4)} = \log\ {}^*K'_{s,(1,4)} + \log\ \gamma_{(1,4)} + \log\ \gamma_{Na^+} + \log\ \gamma_{H^+} - 2.5\ \log\ a_w \quad (11)$$

Experimental solubility data in regions II and III were fitted according to eqs. 8 and 10, and the conditional solubility constants $\log\ {}^*K'_{s,(1,3)}$ and $\log\ {}^*K'_{s,(1,4)}$ determined for I = 0.1, 0.5, 1.0, 2.5, and 5.0 M NaCl (see Table 2). The table also includes the extrapolation to I = 0 as calculated by the SIT and Pitzer approaches. A detailed discussion of the SIT and Pitzer model development within this work is given below.

Table 2 Conditional solubility constants log $^{*}K'_{s,(1,3)}$ and log $^{*}K'_{s,(1,4)}$ (molal scale) for the reactions 0.5 $Na_2Np_2O_7$(cr) + 1.5 $H_2O \Leftrightarrow Na^+ + NpO_2(OH)_3^-$ and 0.5 $Na_2Np_2O_7$(cr) + 2.5 $H_2O \Leftrightarrow Na^+ + NpO_2(OH)_4^{2-} + H^+$. Extrapolation to $I = 0$ are calculated with the SIT and Pitzer approaches.

[NaCl]			
mol·L^{-1}	mol·kg^{-1}	log $^{*}K'_{s,(1,3)}$	log $^{*}K'_{s,(1,4)}$
0.1	0.10	–8.40 ± 0.08	–18.80 ± 0.03
0.5	0.51	–8.05 ± 0.09	–18.35 ± 0.03
1.0	1.02	–7.90 ± 0.18	–18.21 ± 0.02
2.5	2.61	–7.70 ± 0.08	–18.05 ± 0.02
5.0	5.61	–7.15 ± 0.12	–18.40 ± 0.05
$I = 0$		log $^{*}K^{\circ}_{s,(1,3)}$	log $^{*}K^{\circ}_{s,(1,4)}$
SIT		–8.6 ± 0.1	–19.4 ± 0.1
Pitzer		–8.5 ± 0.1	–19.4 ± 0.1

SIT approach

Based on the SIT, the activity coefficient γ_i of an aqueous species i can be calculated with the simple expression [5,27]

$$\log \gamma_i = -z_i^2 D + \Sigma\varepsilon(i,k) m_k \tag{12}$$

where z_i is the charge of ion i, $\varepsilon(i,k)$ is the interaction parameter for a pair of oppositely charged ions, m_k (mol·kg^{-1} H_2O) is the molal concentration of ion k, D is the Debye–Hückel term, and I_m is the molal ionic strength. If the activity coefficients in eqs. 9 and 11 are described with the SIT, the ionic strength dependence of log $^{*}K'_{s,(1,3)}$ and log $^{*}K'_{s,(1,4)}$ for the solubility reactions 6 and 7 is given by eqs. 13 and 14

$$\log {}^{*}K'_{s,(1,3)} = \log {}^{*}K^{\circ}_{s,(1,3)} + 2\,D + 1.5 \log a_w - \varepsilon[NpO_2(OH)_3^-, Na^+]\, m_{Na^+} - \varepsilon(Na^+, Cl^-)\, m_{Cl^-} \tag{13}$$

$$\log {}^{*}K'_{s,(1,4)} = \log {}^{*}K^{\circ}_{s,(1,4)} + 6\,D + 2.5 \log a_w - \varepsilon[NpO_2(OH)_4^{2-}, Na^+]\, m_{Na^+} - \varepsilon(Na^+, Cl^-)\, m_{Cl^-} - \varepsilon(H^+, Cl^-)\, m_{Cl^-} \tag{14}$$

The linear regression of log $^{*}K'_{s,(1,x)} - \Delta z^2 - n \log a_w$ vs. $I_m = m_{NaCl}$ leads to the determination of log $^{*}K^{\circ}_{s,(1,3)} = -8.6 \pm 0.1$ and log $^{*}K^{\circ}_{s,(1,4)} = -19.4 \pm 0.1$ as y-axis intercepts. The slope in both SIT plots ($-\Delta\varepsilon$) combined with $\varepsilon(H^+, Cl^-) = 0.12 \pm 0.01$ mol·kg^{-1} and $\varepsilon(Na^+, Cl^-) = 0.03 \pm 0.01$ mol·kg^{-1} [5] results in $\varepsilon[NpO_2(OH)_3^-, Na^+] = -0.20 \pm 0.02$ mol·kg^{-1} and $\varepsilon[NpO_2(OH)_4^{2-}, Na^+] = -0.12 \pm 0.01$ mol·kg^{-1} (Fig. 6a). SIT ion interaction coefficients correlate with the charge of the species and strongly depend on the corresponding counterion of the background electrolyte (see [8,47]). The value $\varepsilon(NpO_2(OH)_4^{2-}, Na^+) = -0.12 \pm 0.01$ mol·kg^{-1} determined in this work agrees well with the SIT ion interaction coefficient expected for a divalent anion in a Na_2X solution (-0.10 ± 0.10, see [47]). The more negative value determined for $\varepsilon[NpO_2(OH)_3^-, Na^+]$ is in excellent agreement with $\varepsilon[UO_2(OH)_3^-, Na^+]$ determined in Altmaier et al. (2003) [37] (-0.23 ± 0.09 mol·kg^{-1}), although lower values would be expected from a charge-based approximation.

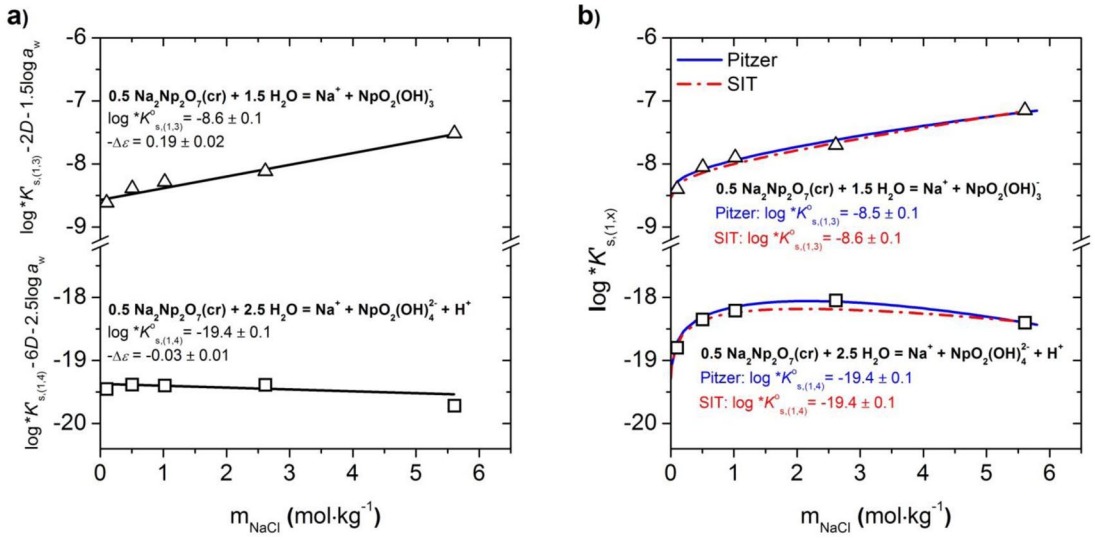

Fig. 6 Determination of log $*K^{\circ}_{s,(1,3)}$ and log $*K^{\circ}_{s,(1,4)}$; (a) extrapolation to $I = 0$ by linear SIT regression; (b) conditional equilibrium constants log $*K'_{s,(1,3)}$ and log $*K'_{s,(1,4)}$ as a function of the NaCl molality; experimental data and calculated functions based on the SIT (dashed lines) and Pitzer approaches (solid lines).

Pitzer approach

The application of the SIT model is normally limited to $I \leq 3.5$ mol·kg^{-1} H_2O, and the use of the Pitzer formulism is required to assess the highly saline conditions of this study. The ion interaction approach of Pitzer was therefore used to derive log $*K^{\circ}_{s,(1,3)}$ and log $*K^{\circ}_{s,(1,4)}$. The Pitzer approach describes the interactions between cation c and anion a by the binary parameters $\beta^{(0)}_{ca}$, $\beta^{(1)}_{ca}$, and C^{φ}_{ca}, whereas the mixing parameters θ_{cc} (or θ_{aa}) and $\psi_{cc'a}$ (or $\psi_{aa'c}$) account for interactions with further cations c (or anions a) in ternary or higher multicomponent electrolyte solutions. The values of log γ_{Na^+}, log γ_{H^+} and log a_w in eqs. 9 and 11 are calculated from the parameters reported by Harvie et al. [48]. $\beta^{(0)}$ and $\beta^{(1)}$ for the species $NpO_2(OH)_3^-$ and $NpO_2(OH)_4^{2-}$ are considered as fitting parameters, whereas C^{φ}_{ca} are set equal to 0. The mixing parameters θ_{aa} and $\psi_{aa'c}$ are set equal to zero as well because they cannot be separated from the binary parameters. The fit is achieved by minimizing the difference between experimental and calculated log $*K'_{s,(1,n)}$ using the Solver tool of Microsoft Excel®. From the equilibrium constants log $*K'_{s,(1,3)}$ and log $*K'_{s,(1,4)}$ in 0.1–5.0 M NaCl, the values of log $*K^{\circ}_{s,(1,3)} = -8.5 \pm 0.1$, log $*K^{\circ}_{s,(1,4)} = -19.4 \pm 0.1$ and the following Pitzer parameters for the cation–anion pairs [Na^+, $NpO_2(OH)_3^-$] and [Na^+, $NpO_2(OH)_4^{2-}$] are calculated (see Fig. 6b).

$$\beta^{(0)}_{Na^+,NpO_2(OH)_3^-} = -0.22 \text{ kg·mol}^{-1}, \qquad \beta^{(1)}_{Na^+,NpO_2(OH)_3^-} = 0.4 \text{ kg·mol}^{-1},$$

$$\beta^{(0)}_{Na^+,NpO_2(OH)_4^{2-}} = -0.03 \text{ kg·mol}^{-1}, \qquad \beta^{(1)}_{Na^+,NpO_2(OH)_4^{2-}} = 1.1 \text{ kg·mol}^{-1}$$

$\beta^{(0)}$ values determined in this work for $NpO_2(OH)_3^-$ and $NpO_2(OH)_4^{2-}$ agree well with estimates based on SIT ion interaction coefficients as indicated in Grenthe et al. (1997) [49] ($\beta^{(0)}_{Na^+,NpO_2(OH)_3^-} = 0.035 + \varepsilon_{Na^+,NpO_2(OH)_3^-}$ (ln 10) / 2 = –0.20 and $\beta^{(0)}_{Na^+,NpO_2(OH)_4^{2-}} = 0.15 + \varepsilon_{Na^+,NpO_2(OH)_4^{2-}}$ (ln 10) / 2 = 0.01). Furthermore, $\beta^{(1)}$ values agree within the uncertainties with typical $\beta^{(1)}$ values reported for 1:1 (0.20 ± 0.20) and 1:2 (1.4 ± 0.6) electrolytes [49].

The ionic strength dependence of log $*K'_{s,(1,3)}$ and log $*K'_{s,(1,4)}$ is shown in Fig. 6b. The figure shows that both SIT and Pitzer approaches reproduce very well log $*K'_{s,(1,n)}$ values determined experimentally up to 5.0 M NaCl, although the Pitzer model is slightly more accurate than the SIT approach

for 2.5 M NaCl. It is also noteworthy that log $^*K^\circ_{s,(1,3)}$ determined by Pitzer is 0.1 log-units more positive than the corresponding constant extrapolated by SIT. The Np solubility calculated with the Pitzer model is shown as solid lines in Fig. 1.

Reductive dissolution of $Na_2Np_2O_7$(cr) and $NpO_2(OH)_2{\cdot}H_2O$(cr)

Aqueous-phase analysis and solid phase characterization detailed in the previous sections indicated that the reductive dissolution of $Na_2Np_2O_7$(cr) and $NpO_2(OH)_2{\cdot}H_2O$(cr) to NpO_2^+ takes place in the near-neutral to slightly alkaline pH range of the solubility curves (region I in Figs. 1a–e). The time-dependence observed in this region for E_h (see Fig. 2) is interpreted in terms of NaClO degradation, which leads further towards a redox-unbuffered system where no reliable E_h values can be measured with combination Pt electrodes. This fact hinders the determination of thermodynamic data based on the redox solubility reactions 3 and 4, where pe values need to be accounted for.

The reduction of Np(VI) to Np(V) is a one-electron transfer reaction involving no structural changes in the neptunyl moiety, and it is thus assumed to rapidly reach a thermodynamic equilibrium. This is further confirmed by the different slopes observed in region I of the solubility curves in 0.1 M NaCl [slope ~ –2, complete transformation to $NpO_2(OH)_2{\cdot}H_2O$(cr)] and 0.5–5.0 M NaCl [slope ~ –3, predominance of $Na_2Np_2O_7$(cr)], which indicates that the equilibrium between the solid and aqueous phases has been attained. Hence, the observed solid phase transformation can be described as a thermodynamic equilibrium independent of E_h and only function of pH_m and $[Na^+]$ (reaction 5; eqs. 15 and 16).

$$\log {}^*K'_{s,0}[0.5\ Na_2Np_2O_7(cr)] - pH_m = \log {}^*K'_{s,0}[NpO_2(OH)_2{\cdot}H_2O(cr)] + \log [Na^+] \quad (15)$$

and

$$\log {}^*K^\circ_{s,0}[0.5\ Na_2Np_2O_7(cr)] + 1.5 \log a_w - pH_m + \log \gamma_{H^+} = \log {}^*K^\circ_{s,0}[NpO_2(OH)_2{\cdot}H_2O(cr)] + \log [Na^+] + \log \gamma_{Na^+} \quad (16)$$

This solid phase transformation is favored at lower pH_m and $[Na^+]$, and is only complete (under the conditions of this study) in 0.1 M NaCl and pH_m = 7.6, where the predominance of $NpO_2(OH)_2{\cdot}H_2O$(cr) is confirmed by XRD. Accounting for the sensitivity of the XRD technique, the content of $Na_2Np_2O_7$(cr) at this pH_m is considered ≤ 5 %. Given the pH dependence in eq. 15, the conversion of one phase into the other is complete within 1 pH-unit: at pH_m = 7.6 and 8.6, [Np] will be 3 times (0.5 log-units) below the solubility of $Na_2Np_2O_7$(cr) and $NpO_2(OH)_2{\cdot}H_2O$(cr), respectively. The point of phase transition is thus pH_m = 8.1, where the Np solid phase is 50 % $Na_2Np_2O_7$(cr) and 50 % $NpO_2(OH)_2{\cdot}H_2O$(cr). A large estimated error (±1.0) has been assigned to this pH_m to account for the inherent uncertainty of the approach.

The relationship between both solubility products is given as log $^*K'_{s,0}[0.5\ Na_2Np_2O_7(cr)]$ = log $^*K'_{s,0}[NpO_2(OH)_2{\cdot}H_2O(cr)]$ + 7.1. It can be extrapolated to I = 0 by SIT as log $^*K^\circ_{s,0}[0.5\ Na_2Np_2O_7(cr)]$ = log $^*K^\circ_{s,0}[NpO_2(OH)_2{\cdot}H_2O(cr)]$ + 7.1 by considering $\varepsilon(H^+, Cl^-)$ = 0.12 ± 0.01 mol·kg^{-1}, $\varepsilon(Na^+, Cl^-)$ = 0.03 ± 0.01 mol·kg^{-1} and a_w as reported in [5].

The NEA-TDB selected a log $^*K^\circ_{s,0}$ = 5.47 ± 0.40 for the solid phase $NpO_3{\cdot}H_2O$(cr) [5], acknowledging that one or more of the other solids reported in the Np(VI) oxo-hydroxide system [$NpO_3{\cdot}2H_2O$, $NpO_2(OH)_2{\cdot}H_2O$, $NpO_3{\cdot}4H_2O$] are likely similar in stability. For the analogous Pu(VI) system, a similar value (log $^*K^\circ_{s,0}$ = 5.5 ± 1.0) was selected for the phase $PuO_2(OH)_2{\cdot}H_2O$(cr). A log $^*K^\circ_{s,0}$ = 4.81 ± 0.43 was originally selected by Grenthe and co-workers for methaschoepite ($UO_3{\cdot}2H_2O$) [22]. The re-evaluation of this data in combination with later experimental studies led in [5] to a weighted average of log $^*K^\circ_{s,0}$ = 5.29 ± 0.01, although the authors finally retained the original selection in [22]. The discussion above highlights that (a) An(VI) oxo-hydroxides solids with similar stability constants exist along the actinide series (U–Np–Pu), in contrast to observations made for An(IV) [50] and (b) different oxo-hydroxides [of a given An(VI)] with different degrees of hydration have similar solubility products. Hence, considering log $^*K'_{s,0}[NpO_2(OH)_2{\cdot}H_2O(cr)]$ ≅ log

$^{*}K'_{s,0}(NpO_3{\cdot}H_2O) = 5.47 \pm 0.40$ and according to eq. 16, a log $^{*}K^{\circ}_{s,0}$ can be calculated for the solubility reaction

$$0.5\ Na_2Np_2O_7(cr) + 3\ H^+ \Leftrightarrow Na^+ + NpO_2^{2+} + 1.5\ H_2O \quad (17)$$

with log $^{*}K^{\circ}_{s,0} = 12.6 \pm 1.1$.

The combination of reaction 17 with reactions 6 and 7, and the corresponding log $^{*}K^{\circ}_{s,(1,3)}$ and log $^{*}K^{\circ}_{s,(1,4)}$ as determined by SIT, allows the calculation of the formation constants for the hydrolysis species $NpO_2(OH)_3^-$ and $NpO_2(OH)_4^{2-}$ (see eqs. 18 and 19). Despite the good experimental accuracy achieved for log $^{*}K^{\circ}_{s,(1,3)}$ and log $^{*}K^{\circ}_{s,(1,4)}$, log $^{*}\beta^{\circ}_{(1,3)}$ and log $^{*}\beta^{\circ}_{(1,4)}$ retain a large uncertainty due to the error assigned to log $^{*}K^{\circ}_{s,0}[0.5\ Na_2Np_2O_7(cr)]$.

$$NpO_2^{2+} + 3\ H_2O \Leftrightarrow NpO_2(OH)_3^- + 3\ H^+ \qquad \log\ ^{*}\beta^{\circ}_{(1,3)} = -21.2 \pm 1.1 \quad (18)$$

$$NpO_2^{2+} + 4\ H_2O \Leftrightarrow NpO_2(OH)_4^{2-} + 4\ H^+ \qquad \log\ ^{*}\beta^{\circ}_{(1,4)} = -32.0 \pm 1.1 \quad (19)$$

Log $^{*}\beta^{\circ}_{(1,4)}$ determined in this work is in good agreement with the corresponding U(VI) analogue (log $^{*}\beta^{\circ}_{(1,4)} = -32.40 \pm 0.68$ [5]) and Np(VI) estimate reported in [14] based on correlations with Z_{eff} (log $^{*}\beta^{\circ}_{(1,4)} = -31.6 \pm 1.0$). Although overlapping within their (large) uncertainties, log $^{*}\beta^{\circ}_{(1,3)}$ determined in this work falls clearly below the stability constants for the U(VI) analogue (log $^{*}\beta^{\circ}_{(1,3)} = -20.25 \pm 0.42$ [5]) and Np(VI) estimate (log $^{*}\beta^{\circ}_{(1,3)} = -19.6 \pm 1.0$ [14]).

The authors want to point out that in order to keep the internal consistency in future thermodynamic calculations, log $^{*}\beta^{\circ}_{(1,3)}$ and log $^{*}\beta^{\circ}_{(1,4)}$ determined in this work should only be used in combination with log $^{*}K^{\circ}_{s,0}[0.5\ Na_2Np_2O_7(cr)]$ and log $^{*}K^{\circ}_{s,0}[NpO_2(OH)_2{\cdot}H_2O(cr)]$ values also reported here.

Understanding the behavior of Np under alkaline conditions: Implications of the new Np(VI) thermodynamic data

The chemical and thermodynamic models developed in this work for Np(VI) solubility and speciation in NaCl media were combined with the NEA-TDB data selection for Np (see Tables 3 and 4) to assess the chemical (redox) speciation of this actinide under near-neutral to hyperalkaline conditions covering the complete stability field of water (Fig. 7). Thermodynamic calculations were performed for dilute (0.1 M, thick solid lines) and concentrated (5.0 M, thick dashed lines) NaCl solutions, assessing both aqueous speciation and solid phase formation. The NaCl concentrations chosen for the calculations are representative of cementitious environments (~0.12 M Na^+ in porewater of fresh cement [4]) and brines in salt-rock repositories (~5 M Na^+, in the unlikely scenario of water intrusion [2,3]).

As expected, calculations based upon the improved thermodynamic description derived in this work show that Np(IV) aqueous species and solid compounds prevail in the strongly reducing conditions characteristic of a deep underground nuclear waste repository. Under mildly reducing to oxidizing conditions, Np(V) predominates in the aqueous phase at pH_m values below ~10. Above this pH_m, the stability field of aqueous Np(VI) species increases due to the formation of $NpO_2(OH)_3^-$ and $NpO_2(OH)_4^{2-}$ complexes. These species become more stable under redox neutral conditions ("redox neutral line") at pH_m ~13.5 and outcompete Np(V) (with a lower tendency to hydrolyze).

The $Na_2Np_2O_7(cr)$ phase newly identified in this work as the solubility-limiting solid phase in NaCl solution is favored over $NpO_2OH(am, fresh)$ in both NaCl 0.1 M and 5.0 M, directly defining a borderline with $NpO_2(am, hyd)$ at $pH_m \geq$ ~11 (see Fig. 7b). It should be noted, however, that recent investigations by Petrov and co-workers [35] indicate the formation of stable Na–Np(V) solid phases at $pH_m \geq 11.8$ and $I \geq 1.0$ M NaCl, although no thermodynamic data for these solids were reported so far. The incorporation of these compounds in the thermodynamic calculations shown in Fig. 7 may affect the picture of redox distribution for solid phases under saline conditions.

Table 3 Stability constants (I = 0, 298.15 K) for the formation of aqueous species and solid compounds of Np reported in the NEA-TDB and determined in the present work. Only species forming within $6 < pH_m < 14$ are considered.

Hydrolysis and redox reactions	log $*\beta^\circ$	Ref.
$NpO_2^+ + 4\ H^+ + e^- \Leftrightarrow Np^{4+} + 2\ H_2O$	10.21 ± 1.39	[5]
$Np^{4+} + 4\ H_2O \Leftrightarrow Np(OH)_4(aq) + 4\ H^+$	–8.3 ± 1.1	[5]
$NpO_2^{2+} + e^- \Leftrightarrow NpO_2^+$	19.59 ± 1.39	[5]
$NpO_2^+ + H_2O \Leftrightarrow NpO_2OH(aq) + H^+$	–11.3 ± 0.7	[5]
$NpO_2^+ + 2\ H_2O \Leftrightarrow NpO_2(OH)_2^- + 2\ H^+$	–23.6 ± 0.5	[5]
$NpO_2^{2+} + H_2O \Leftrightarrow NpO_2OH^+ + H^+$	–5.1 ± 0.4	[5]
$2\ NpO_2^{2+} + 2\ H_2O \Leftrightarrow (NpO_2)_2(OH)_2^{2+} + 2\ H^+$	–6.27 ± 0.21	[5]
$3\ NpO_2^{2+} + 5\ H_2O \Leftrightarrow (NpO_2)_3(OH)_5^+ + 5\ H^+$	–17.12 ± 0.22	[5]
$NpO_2^{2+} + 3\ H_2O \Leftrightarrow NpO_2(OH)_3^- + 3\ H^+$	–21.2 ± 1.1	[p.w.]
$NpO_2^{2+} + 4\ H_2O \Leftrightarrow NpO_2(OH)_4^{2-} + 4\ H^+$	–32.0 ± 1.1	[p.w.]
Solubility reactions	**log $*K^\circ_{s,0}$**	
$NpO_2(am, hyd) + 4\ H^+ \Leftrightarrow Np^{4+} + 2\ H_2O$	–0.7 ± 0.5	[5]
$NpO_2OH(am, fresh) + H^+ \Leftrightarrow NpO_2^+ + H_2O$	5.3 ± 0.2	[5]
$NpO_3{\cdot}H_2O(cr) + 2\ H^+ \Leftrightarrow NpO_2^{2+} + 2\ H_2O$	5.47 ± 0.40	[5]
$NpO_2(OH)_2{\cdot}H_2O(cr) + 2\ H^+ \Leftrightarrow NpO_2^{2+} + 3\ H_2O$	5.47 ± 0.40[a]	[p.w.]
$0.5\ Na_2Np_2O_7(cr) + 3\ H^+ \Leftrightarrow NpO_2^{2+} + Na^+ + 1.5\ H_2O$	12.6 ± 1.1	[p.w.]

[a]Same log $*K^\circ_{s,0}$ as $NpO_3{\cdot}H_2O(cr)$.

Table 4 SIT coefficients (i,k) [kg·mol^{-1}] for Np(IV/V/VI) species in NaCl media at 298.15 K.

i	k	$\varepsilon(i,k)$ [mol·kg^{-1}]	Ref.
NpO_2^+	Cl^-	(0.09 ± 0.05)	[5]
NpO_2OH^+	Cl^-	(0.05 ± 0.10)	a
$(NpO_2)_3(OH)_5^+$	Cl^-	(0.81 ± 0.17)	b
NpO_2^{2+}	Cl^-	(0.15 ± 0.10)	a
$(NpO_2)_2(OH)_2^{2+}$	Cl^-	(0.69 ± 0.07)	b
Np^{4+}	Cl^-	(0.35 ± 0.10)	a
$Np(OH)_4(aq)$	Cl^-/Na^+	0	c
$NpO_2OH(aq)$	Cl^-/Na^+	0	c
$NpO_2(OH)_2^-$	Na^+	(–0.05 ± 0.05)	a
$NpO_2(OH)_3^-$	Na^+	(–0.20 ± 0.02)	[p.w.]
$NpO_2(OH)_4^{2-}$	Na^+	(–0.12 ± 0.01)	[p.w.]

[a]Estimated by correlation with Z according to [47].
[b]Analogy with U(VI).
[c]By definition set to zero in SIT.

The results discussed above relate to the understanding of the retention processes of Np in cementitious and saline environments under anoxic to oxidizing conditions. In view of the recent sorption and spectroscopic studies [15,16], Np(VI) is expected to sorb weakly onto cementitious materials at pH ~ 13.3 (R_d ~10^3 L·kg^{-1}) in contrast to Np(V) (R_d ~10^6 L·kg^{-1}). A similar behavior was reported for the uptake of U(VI) by calcium silicate hydrates (C–S–H phases) and cement [52–55]. Whether interpreted as a surface complexation process [53] or as a solid solution formation with the C–S–H phases [55], the weak sorption of An(VI) is likely related to the formation of highly charged anions under hyperalkaline

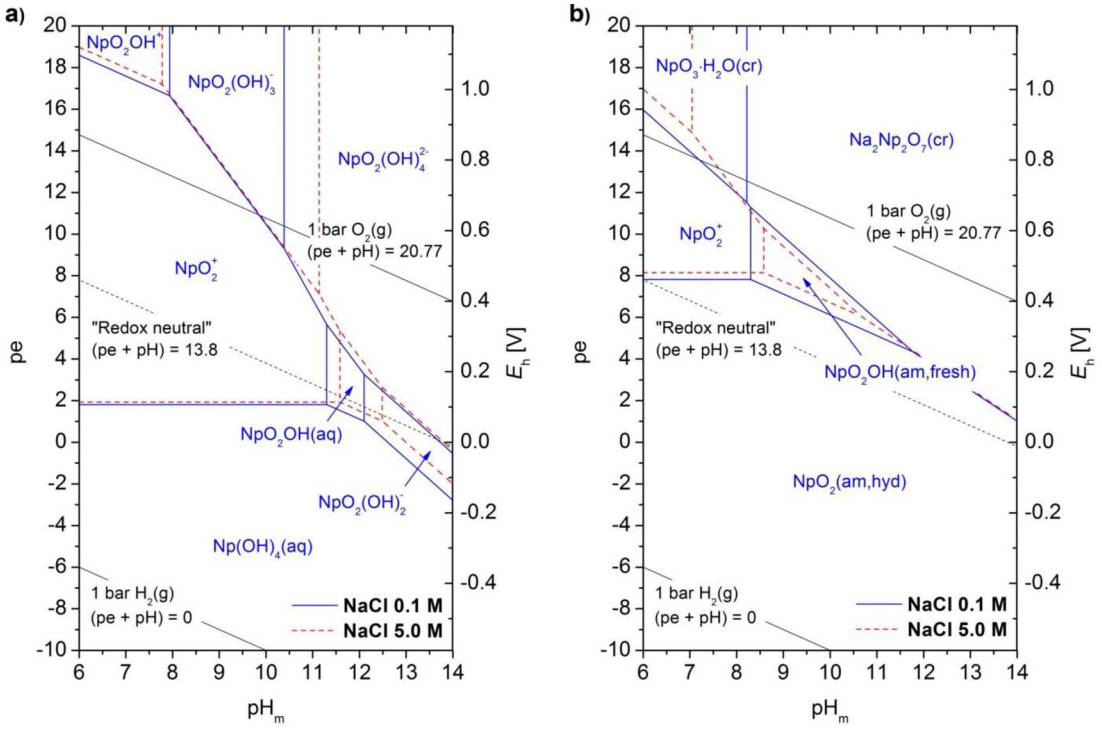

Fig. 7 Predominance diagram of aqueous Np species (a) and solid Np compounds (b) under near-neutral to hyperalkaline pH conditions. Calculations performed with thermodynamic data for Np summarized in Table 3 and $[Np]_{tot} = 1 \times 10^{-3}$ M. Log $*\beta^\circ$ and log $*K_{s,0}$ values were recalculated to $I = 0.1$ and 5.0 M by SIT considering $\varepsilon(i,k)$ values in Table 4. Calculations were performed with the code Medusa [51].

conditions [$AnO_2(OH)_4^{2-}$] and the lower tendency of these species to interact with negatively charged silanol surfaces. On the other hand, the stabilization of the crystalline Np(VI) phase $Na_2Np_2O_7$(cr) sets very low solubility limits within the pH_m range 9–11 ([Np] ~10^{-8} M), in contrast to the much higher solubility imposed by the corresponding Np(V) solid NpO_2OH(am, fresh) (~10^{-4}–10^{-6} M).

CONCLUSIONS

The formation and stability of aqueous and solid Np(VI) species in the alkaline pH range is confirmed for anoxic to oxidizing conditions in dilute to concentrated carbonate-free NaCl solutions. Based on solubility experiments and detailed solid phase characterization, a chemical model has been developed including Np(VI) aqueous species [$NpO_2(OH)_3^-$ and $NpO_2(OH)_4^{2-}$] and solid compounds [$Na_2Np_2O_7$(cr) and $NpO_2(OH)_2 \cdot H_2O$(cr)] not considered in the NEA-TDB. These aqueous species and solid compounds are analogous to those previously described for U(VI), as expected from the concept of chemical analogy for actinides of the same redox state. The SIT and Pitzer approaches are used to extrapolate the conditional stability constants determined in 0.1–5.0 M NaCl to $I = 0$ and to determine the corresponding ion interaction parameters.

The newly determined thermodynamic data close an important data gap affecting the aqueous chemistry of Np under alkaline and anoxic to oxidizing conditions, which can be now reliably calculated for dilute to concentrated NaCl solutions. The improved picture of Np redox chemistry and redox stability derived in this work indicates the need to accurately evaluate Np redox behavior and specia-

tion in specific nuclear waste disposal scenarios where the formation of the +VI redox state can affect the mobilization/retention processes currently predicted for Np.

ACKNOWLEDGMENTS

V. Petrov (Moscow State University) is kindly acknowledged for the preparation of the ^{237}Np stock solution. The contribution of M. Böttle and E. Soballa (KIT-INE) to ICP-OES and SEM-EDS analysis is highly appreciated. M. Ernstberger and T. Wiss (JRC-ITU) are gratefully acknowledged for the TG-DTA analysis. Special thanks are due to J. Tits, E. Wieland (Paul Scherrer Institut), and V. Neck (†) for stimulating discussions on Np chemistry under hyperalkaline conditions. The research leading to these results has received funding from the European Union's European Atomic Energy Community's (Euratom) Seventh Framework Programme FP7/2007–2011 under grant agreement n° 212287 (RECOSY project).

REFERENCES

1. M. Altmaier, V. Metz, V. Neck, R. Müller, T. Fanghänel. *Geochim. Cosmochim. Acta* **67**, 3595 (2003).
2. D. T. Reed, J. F. Lucchini, S. B. Aase, A. J. Kropf. *Radiochim. Acta* **94**, 591 (2006).
3. M. Altmaier, C. Bube, B. Kienzler, V. Metz, D. T. Reed. "Proceedings of the International Workshop ABC-Salt (II) and HiTAC", in *ABC-Salt (II) and HiTAC*, Karlsruhe, Germany (2011).
4. E. Wieland, L. R. Van Loon. "Cementitious near-field sorption database for performance assessment of an ILW repository in Opalinus clay", Nagra Technical Report NTB 02-20, Nagra, Wettingen, Switzerland (2002).
5. R. Guillaumont, J. Fanghänel, V. Neck, J. Fuger, D. A. Palmer, I. Grenthe, M. H. Rand. *Chemical Thermodynamics, Vol. 5, Update on the Chemical Thermodynamics of Uranium, Neptunium, Plutonium, Americium and Technetium*, OECD, NEA-TDB, Elsevier, North Holland, Amsterdam (2003).
6. A. Olin, B. Noläng, L. O. Öhman, E. Osadchii, E. Rosen. *Chemical Thermodynamics, Vol. 7, Chemical Thermodynamics of Selenium*, OECD, NEA-TDB, Elsevier, North Holland, Amsterdam (2005).
7. P. L. Brown, E. Curti, B. Grambow. *Chemical Thermodynamics, Vol. 8, Chemical Thermodynamics of Zirconium*, OECD, NEA-TDB, Elsevier, North Holland, Amsterdam (2005).
8. M. Rand, J. Fuger, I. Grenthe, V. Neck, D. Rai. *Chemical Thermodynamics, Vol. 11, Chemical Thermodynamics of Thorium*, OECD, NEA-TDB, Elsevier, North Holland, Amsterdam (2009).
9. H. Moriyama, M. I. Pratopo, K. Higashi. *Radiochim. Acta* **69**, 49 (1995).
10. A. Cassol, G. Tomat, R. Portanov, L. Magon. *Inorg. Chem.* **11**, 515 (1972).
11. G. R. Choppin, E. N. Rizkalla. "Solution chemistry of actinides and lanthanides", in *Handbook on the Physics and Chemistry of Rare Earths*, K. A. Gschneidner Jr., L. Eyring (Eds.), North Holland, Amsterdam (1994).
12. G. R. Choppin. *Radiochim. Acta* **85**, 89 (1999).
13. R. J. Lemire, J. Fuger, H. Nitsche, P. E. Potter, M. H. Rand, J. Rydberg, K. Spahiu, J. C. Sullivan, W. J. Ullman, P. Vitorge, H. Wanner. *Chemical Thermodynamics, Vol. 4, Neptunium and Plutonium*, OECD, NEA-TDB, Elsevier, North Holland, Amsterdam (2001).
14. X. Gaona, J. Tits, K. Dardenne, X. Liu, J. Rothe, M. A. Denecke, E. Wieland, M. Altmaier. *Radiochim. Acta* **100**, 759 (2012).
15. X. Gaona, E. Wieland, J. Tits, A. C. Scheinost, R. Dähn. *Appl. Geochem.* **28**, 109 (2013).
16. J. Tits, X. Gaona, A. Laube, E. Wieland. "Influence of the redox state on the neptunium sorption by cementitious materials", in *ReCosy 3rd Annual Workshop*, Balaruc-les-Bains, France (2011).
17. K. W. Bagnall, J. B. Laidler. *J. Chem. Soc.* 2693 (1964).

18. Y. Kato, T. Kimura, Z. Yoshida, N. Nitani. *Radiochim. Acta* **74**, 21 (1996).
19. D. Cohen. *Inorg. Chem.* **2**, 866 (1963).
20. T. Saito, J. Wang, T. Kitazawa, M. Takahashi, M. Takeda, M. Nakada, T. Nakamoto, N. M. Masaki, T. Yamashita, M. Saeki. *J. Radioanal. Nucl. Chem.* **239**, 319 (1999).
21. M. Nakada, T. Kitazawa, T. Saito, J. H. Wang, M. Takeda, T. Yamashita, M. Saeki. *Bull. Chem. Soc. Jpn.* **76**, 1375 (2003).
22. I. Grenthe, J. Fuger, R. J. M. Konings, R. J. Lemire, A. B. Muller, C. Nguyen-Trung, H. Wanner. *Chemical Thermodynamics, Vol. 1, Chemical Thermodynamics of Uranium*, OECD, NEA-TDB, Elsevier, North Holland, Amsterdam (1992).
23. J. Goudiakas, X. Jemine, J. Fuger. *J. Chem. Thermodyn*. **23**, 513 (1991).
24. J. Fuger. *J. Nucl. Mater.* **130**, 253 (1985).
25. V. Neck, M. Altmaier, T. Fanghänel. *C. R. Chim.* **10**, 959 (2007).
26. V. Neck, M. Altmaier, A. Seibert, J. I. Yun, C. M. Marquardt, T. Fanghanel. *Radiochim. Acta* **95**, 193 (2007).
27. L. Ciavatta. *Ann. Chim. (Rome)* **70**, 551 (1980).
28. K. S. Pitzer. *J. Phys. Chem*. **77**, 268 (1973).
29. K. S. Pitzer. *Activity Coefficients in Electrolyte Solutions*, CRC Press, Boca Raton (1991).
30. I. Pashalidis, J. I. Kim, C. Lierse, J. C. Sullivan. *Radiochim. Acta* **60**, 99 (1993).
31. W. H. Kim, K. C. Choi, K. K. Park, T. Y. Eom. *Radiochim. Acta* **66–67**, 45 (1994).
32. I. Grenthe, W. Stumm, M. Laaksuharju, A. C. Nilsson, P. Wikberg. *Chem. Geol*. **98**, 131 (1992).
33. M. Altmaier, X. Gaona, D. Fellhauer, G. Buckau. "Intercomparison of redox determination methods on designed and near-neutral aqueous systems; KIT-SR 7572", Karlsruhe Institute of Technology, Karlsruhe (2010).
34. V. Neck, W. Runde, J. I. Kim, B. Kanellakopulos. *Radiochim. Acta* **65**, 29 (1994).
35. V. G. Petrov, X. Gaona, D. Fellhauer, K. Dardenne, S. N. Kalmykov, M. Altmaier. "Np(V) solubility and solid phase transformation in dilute to concentrated NaCl solutions", in *Migration Conference*, Beijing (2011).
36. V. Neck, J. L. Kim, B. Kanellakopulos. *Radiochim. Acta* **56**, 25 (1992).
37. M. Altmaier, V. Neck, V. Metz, R. Müller, M. Schlieker, Th. Fanghänel. "Solubility of U(VI) in NaCl and $MgCl_2$ solution", in *Migration Conference*, Gyeongju, Korea (2003).
38. V. I. Spitsyn, A. D. Gelman, N. N. Krot, M. P. Mefodiye, F. A. Zakharov, Y. A. Komkov, V. P. Shilov, I. V. Smirnova. *J. Inorg. Nucl. Chem.* **31**, 2733 (1969).
39. V. P. Shilov, E. S. Stepanov, N. N. Krot. *Radiokhimiya* **19**, 73 (1977).
40. H. Bolvin, U. Wahlgren, H. Moll, T. Reich, G. Geipel, T. Fanghänel, I. Grenthe. *J. Phys. Chem. A* **105**, 11441 (2001).
41. C. W. Williams, J. P. Blaudeau, J. C. Sullivan, M. R. Antonio, B. Bursten, L. Soderholm. *J. Am. Chem. Soc.* **123**, 4346 (2001).
42. D. Clark, P. D. Palmer, C. D. Tait, D. W. Keogh. "Unusual tetraoxo coordination in heptavalent neptunium", *Actinide Research Quarterly*, First Quarter (2004).
43. J. E. C. Wren, G. Schreckenbach. *Can. J. Chem*. **87**, 1436 (2009).
44. D. L. Clark, S. D. Conradson, R. J. Donohoe, D. W. Keogh, D. E. Morris, P. D. Palmer, R. D. Rogers, C. D. Tait. *Inorg. Chem.* **38**, 1456 (1999).
45. H. Moll, T. Reich, Z. Szabo. *Radiochim. Acta* **88**, 411 (2000).
46. C. Keller, L. Koch, K. H. Walter. *J. Inorg. Nucl. Chem.* **27**, 1205 (1965).
47. W. Hummel. "Ionic strength corrections and estimation of SIT ion interaction coefficients; PSI Report TM-44-09-01", Paul Scherrer Institut, Villigen, Switzerland (2009).
48. C. F. Harvie, N. Møller, J. H. Weare. *Geochim. Cosmochim. Acta* **48**, 723 (1984).
49. I. Grenthe, A. V. Plyasunov, K. Spahiu. "Estimations of medium effects on thermodynamic data", in *Modelling in Aquatic Chemistry*, I. Grenthe, I. Puigdomènech (Eds.), NEA/OCDE, Paris (1997).

50. V. Neck, J. I. Kim. *Radiochim. Acta* **89**, 1 (2001).
51. I. Puigdomènech. INPUT, SED, and PREDOM: Computer programs drawing equilibrium diagrams; TRITA-OOK-3010 Royal Institute of Technology (KTH), Dept. Inorg. Chemistry, Stockholm (1983).
52. J. Tits, G. Geipel, N. Macé, M. Eilzer, E. Wieland. *J. Colloid Interface Sci.* **359**, 248 (2011).
53. I. Pointeau, C. Landesman, E. Giffaut, P. Reiller. *Radiochim. Acta* **92**, 645 (2004).
54. I. Pointeau, N. Coreau, P. Reiller. *Radiochim. Acta* **96**, 367 (2008).
55. X. Gaona, D. Kulik, N. Macé, E. Wieland. *Appl. Geochem*. **27**, 91 (2012).

APPENDIX

Solubility data of U(VI) in NaCl solutions reported in Altmaier et al. (2003) [37] compared to present data for Np(VI).

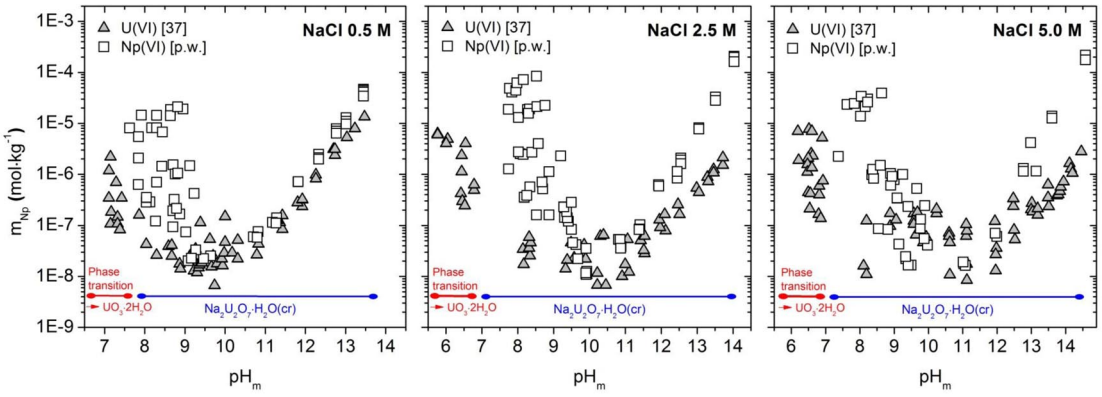

Fig. A1 Comparison of U(VI) and Np(VI) solubility data in 0.5, 2.5, and 5.0 M NaCl reported in Altmaier et al. (2003) [37] and determined in this work, respectively. Solid phases controlling the solubility of U(VI) are indicated in the figure as reported in [37].

